High-quality crystalline yttria-stabilized-zirconia thin layer for photonic applications

Guillaume Marcaud, Sylvia Matzen, Carlos Alonso-Ramos, Xavier Le Roux, Mathias Berciano, Thomas Maroutian, Guillaume Agnus, Pascal Aubert, Ludovic Largeau, Valérie Pillard, Samuel Serna, Daniel Benedikovic, Christopher Pendenque, Eric Cassan, Delphine Marris-Morini, Philippe Lecoeur, and Laurent Vivien
Centre de Nanosciences et Nanotechnologies (C2N), Université Paris-Sud, CNRS UMR 9001, Université Paris-Saclay, Orsay, 91405, France

(Received 29 November 2017; published 26 March 2018)

Functional oxides are considered as promising materials for photonic applications due to their extraordinary and various optical properties. Especially, yttria-stabilized zirconia (YSZ) has a high refractive index (∼2.15), leading to a good confinement of the optical mode in waveguides. Furthermore, YSZ can also be used as a buffer layer to expand toward a large family of oxides-based thin-films heterostructures. In this paper, we report a complete study of the structural properties of YSZ for the development of integrated optical devices on sapphire in telecom wavelength range. The substrate preparation and the epitaxial growth using pulsed-laser deposition technique have been studied and optimized. High-quality YSZ thin films with remarkably sharp x-ray diffraction rocking curve peaks in $10^{-3\circ}$ range have then been grown on sapphire (0001). It was demonstrated that a thermal annealing of sapphire substrate before the YSZ growth allowed controlling the out-of-plane orientation of the YSZ thin film. Single-mode waveguides were finally designed, fabricated, and characterized for two different main orientations of high-quality YSZ (001) and (111). Propagation loss as low as 2 dB/cm at a wavelength of 1380 nm has been demonstrated for both orientations. These results pave the way for the development of a functional oxides-based photonics platform for numerous applications including on-chip optical communications and sensing.

DOI: 10.1103/PhysRevMaterials.2.035202

I. INTRODUCTION

Intensive researches are currently conducted on the miniaturization of photonic devices and on the combination of photonics and electronics to decrease the power consumption and to create novel functionalities for a myriad of applications including datacom, telecom, sensing, and quantum optics, to name a few [1–3]. In this context, functional oxides have emerged as a promising material family to expand the functionalities of current photonic circuits thanks to their wide range of properties as multiferroicity, piezoelectricity, and optical nonlinearities [4–8]. Usually, the epitaxial growth of high-crystalline quality functional oxides requires a buffer layer for a better lattice adaptation and to avoid interdiffusion between substrate and oxide materials. One of these oxides is the yttria-stabilized zirconia (YSZ), extensively used as a buffer layer for $LiNbO_3$, $PbTiO_3$, $Pb(Zr,Ti)O_3$, and $YBa_2Cu_3O_7$ [9–12] integration on silicon and as a solid electrolyte in gas sensors and fuel cells [13–17]. YSZ is also well known for its extraordinary thermal and chemical stability, as well as its hardness and mechanical durability. An increasing quantity of applications uses this material for the combination of its excellent mechanical and optical properties, such as its high refractive index, large optical band gap, and transparency from the ultraviolet to the near-infrared [18–23]. However, none of these works has considered YSZ for integrated optics in thin-films form.

In this work, the design, fabrication, and characterization of low-loss optical waveguides and grating couplers were presented with very promising results in the use of functional oxides for photonic applications. As substrate, *C*-cut sapphire was considered due to its high mechanical and chemical stability and optical transparency [24–27]. The effect of substrate treatment on the orientation and crystallinity of YSZ grown by pulsed-laser deposition (PLD) is studied and the propagation loss of rib optical waveguides reported for two YSZ orientations.

II. EXPERIMENTAL DETAILS

Substrates were either just cleaned in ethanol and acetone solutions or cleaned the same way and annealed at 1200 °C during 4 h in oxygen or nitrogen atmosphere before deposition.

Laser ablation of yttria-stabilized zirconia (8 mol %) rotating ceramic target was carried out in a high-vacuum stainless-steel chamber with a base pressure of 10^{-6} Torr. The target was irradiated at a 45° incidence angle by KrF excimer laser (248-nm wavelength, 3-J/cm² fluence, and 5-Hz repetition rate). The substrate holder was placed at 50 mm from the target and heated to 800 °C during the deposition. The background gas consisted of O_2 at different pressures. Films deposited on sapphire (0001) were then cooled under 300 Torr oxygen at a rate of 10 °C/min.

Film thickness measurements were obtained with spectroscopic ellipsometry (J.A. Woollam). The structural quality and thin-film orientation have been analyzed by high-resolution x-ray diffraction and noncoplanar grazing incidence x-ray diffraction (GIXD) using PANalytical X'Pert Pro and Rigaku Smartlab diffractometers, both in parallel beam configuration with monochromated Cu Kα1 radiation (wavelength of 1.540 598 Å). Finally, cross sections have been realized by focused ion beam (FIB) using an FEI Scios dual beam and then

 ©2018 American Physical Society

observed by transmission electron microscopy (TEM) using an aberration probe-corrected FEI Titan Themis microscope.

III. GROWTH AND STRUCTURAL CHARACTERIZATION

PLD technique has been extensively used for thin-film deposition of complex oxides [18,28,29], essentially because the laser ablation process preserves stoichiometry, enabling good physical properties and high crystallinity of the deposited layer. Laser ablation of ceramic YSZ (8 mol % $Y_2O_3-Y_{0.15}Zr_{0.85}O_{1.93}$) rotating target was carried out in a high-vacuum stainless-steel chamber with a base pressure of 10^{-6} Torr. The target was irradiated at a 45° incidence angle by an excimer laser KrF (248-nm wavelength, 3-J/cm² fluence, and 5-Hz repetition rate).

The thin-film orientation and roughness under different deposition conditions were examined by x-ray diffraction (XRD), TEM, and atomic force microscopy (AFM). As expected, only two out-of-plane orientations (111) and (001) of YSZ thin film on sapphire (0001) have been detected by XRD [30]. In order to promote only one orientation and limit grain boundaries responsible for optical losses, partial oxygen pressure during the growth has been first optimized, and then the effect of surface structure of the substrate has been probed with two different kinds of thermal annealing.

A. Oxygen partial pressure during deposition

From XRD diffraction peaks area, we have defined volume ratios of both (001) and (111) growth orientations. (001) YSZ volume ratio (V_{001}) was estimated from the integral of (002) and (111) x-ray diffraction peaks: $V_{001} = (4 \times \int I_{002})/(\int I_{111} + 4 \times I_{002})$, where structure factor is taken into account and background signal subtracted. $V_{001} = 100\%$ means the crystallized volume is totally (00l) oriented and $V_{001} = 0\%$ totally (hhh) oriented. As a reference, a first set of samples was fabricated using sapphire substrates only cleaned with acetone and ethanol prior to deposition. Volume ratio V_{001} is plotted in Fig. 1 as a function of the total pressure in the deposition chamber. Red points correspond to pure oxygen atmosphere gas and black points to a mixture of Ar/O_2 with an oxygen partial pressure maintained at 30 mTorr. These results reveal that the amount of (001)-oriented grains increases with the oxygen pressure and not with the argon pressure, which is consistent with the work of Fork *et al.* [31] and Wu *et al.* [10] demonstrating that the epitaxy of (001) YSZ on sapphire can only occur when high oxygen pressure is used during the deposition. Dai *et al.* [30] have explained also that the formation of Y–O and Zr–O bonds thanks to the interaction of the plasma with oxygen gas promotes the nucleation of (001) YSZ. Indeed, low oxygen pressure allows the growth of (001) YSZ only if nuclei are properly provided with high oxygen pressure at the early stage. In our study, we noticed that an oxygen pressure about 30 mTorr corresponds to the upper limit for the growth of single (111) orientation of YSZ. This pressure has been then used as a standard atmosphere in the following because it allows us to grow only one orientation (111) of YSZ and prevent oxygen vacancies encountered at lower oxygen pressure.

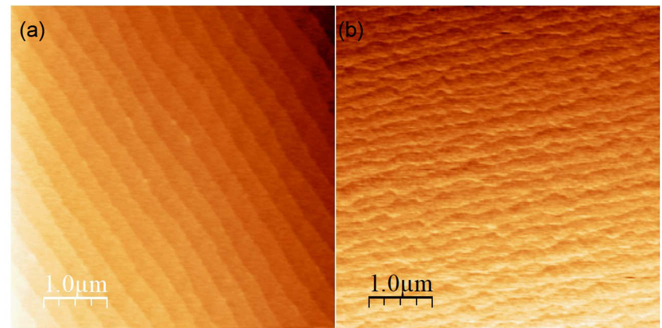

FIG. 2. AFM images of (0001) sapphire surface annealed at 1200 °C during 4 h presenting terrace-step structures. (a) Substrate 1 annealed with nitrogen presents well-defined step of 2-Å height, corresponding to the minimum distance between the oxygen layers in the sapphire lattice (1/6 lattice parameter). (b) Substrate 2 annealed with oxygen leads to step bunching of 2–6 Å and faceted step edges.

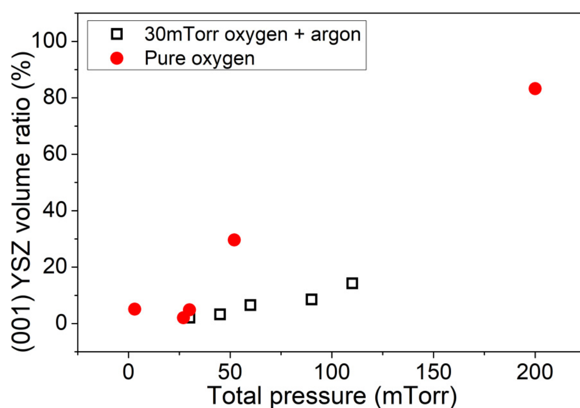

FIG. 1. (001) YSZ volume ratio as a function of total pressure for 3000 pulses of deposition (from 50 to 150-nm-thick layer was deposited depending on the pressure). Pure oxygen (red circles) and a mixture of argon and 30 mTorr of oxygen (black squares) have been used during the growth. Sapphire substrates were only cleaned with ethanol and acetone prior to the deposition.

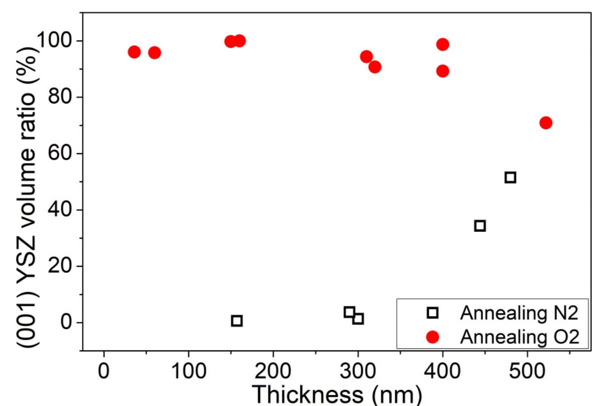

FIG. 3. (001) YSZ volume ratio as a function of the film thickness on sapphire annealed with nitrogen (black squares, substrate 1) or with oxygen (red circles, substrate 2). (001) YSZ volume ratio has been evaluated from the integration of (002) and (111) peaks in x-ray diffraction.

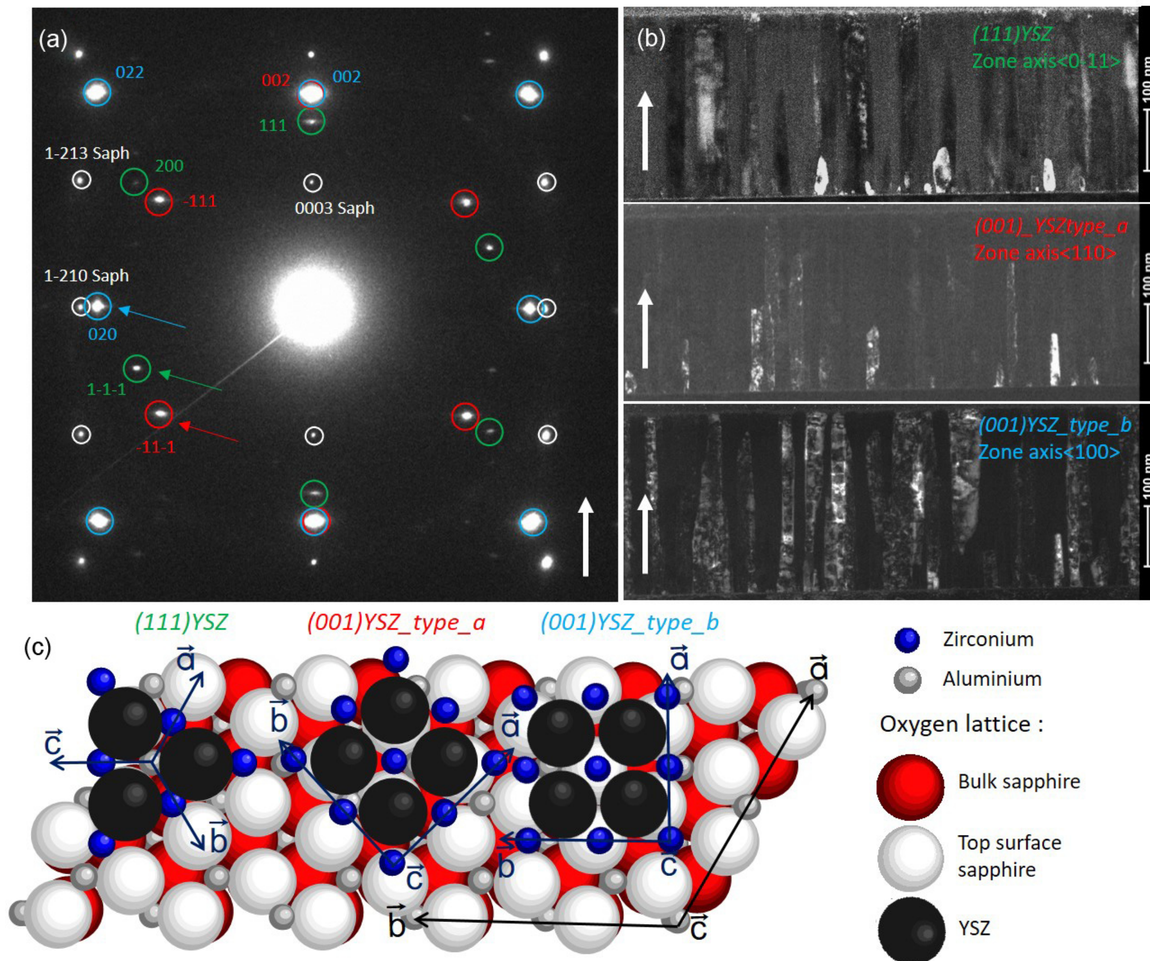

FIG. 4. (a) Electron diffraction of epitaxial YSZ film on (0001) sapphire substrate showing the coexistence of (111) YSZ in green, (001) YSZ type_a in red, and (001) YSZ type_b in blue (250-nm-thick layer) deposited on oxygen-annealed sapphire (substrate 2). (b) DF images represent in bright color the spatial distribution of the different oriented grains in the YSZ layer. These three DF images have been performed thanks to the SAED technique, with objective diaphragm positioned on the electron-diffraction spot marked by an arrow [in (a)] corresponding to YSZ domain of the same color. (c) Schematical top view of relative in-plane orientation of one variant for each corresponding YSZ grain. White arrows represent growth axis on both electron diffraction (a) and DF images (b).

We have then focused our study on preparation of sapphire substrate through two different thermal annealing conditions.

B. Annealing of the substrate

In order to change the surface structure, sapphire substrates have been annealed in an external oven at 1200 °C with either pure nitrogen (substrate 1) or pure oxygen (substrate 2) atmosphere during 4 h. AFM images reported in Fig. 2 after annealing reveal the surface topography of both substrates (1 and 2). Nitrogen annealing always results in well-defined terrace-step structures with 2-Å step height whereas oxygen annealing leads to steps coalescence of 2–6-Å height and faceted step edges.

The YSZ deposition on both substrates 1 and 2 has been performed with 30 mTorr of pure oxygen. Results regarding crystallographic orientation are plotted in Fig. 3 as a function of YSZ film thickness. For the growth of YSZ, a layer with thicknesses up to 300 nm on substrate 1, annealed with nitrogen, gives the same results as with acetone/ethanol cleaning (Fig. 1). YSZ grains are mainly (111) oriented with $V_{001} = 0\%$. For films thicker than 300 nm, the ratio decreases down to $V_{001} \approx 50\%$ for 480-nm-thick film. This transition around 350–400 nm may be due to the lower surface free energy of (001) YSZ planes.

Substrate 2, annealed with oxygen, induces a totally different behavior. Indeed, mainly the (001)-oriented YSZ is grown for the thickness range from 50 to 500 nm. The volume ratio reaches 99% but never 100% due to a residual quantity of (111) YSZ-oriented grains in the layer. The mechanism involved is explained afterward.

Figures 1 and 3 demonstrate that the thin-film orientation is sensitive to the oxygen pressure during the deposition but also highly dependent on preparation of the substrate. Oxygen or nitrogen annealing induces a preferential growth of (001) or (111) YSZ at the same oxygen growth pressure of 30 mTorr, respectively. For a better understanding of the origin of these two orientations, XRD azimuthal scans were performed to determine the epitaxial relations between YSZ and sapphire.

C. In-plane orientation of YSZ on sapphire

In-plane orientation relationships between thin film and sapphire have been determined for both (001) and (111) YSZ out-of-plane orientations using different techniques: XRD azimuthal scans in asymmetric condition, noncoplanar GIXD, and electron diffraction (Fig. 4). Further structural analysis has been performed thanks to the *Z*-contrast imaging of the high-angle annular dark field (HAADF), scanning transmission electron microscopy (STEM), and the different YSZ domains have been located in the layer with the selected area electron-diffraction (SAED) techniques. For both substrates 1 and 2, two variants of (111) YSZ separated by 60° can grow on (0001) sapphire, corresponding to *ABCABC* ... or *CBACBA* ... stacking of the fcc structure of YSZ:

$$(111)_{\mathrm{YSZ}}//(0001)_{\mathrm{saph}}:$$

$$[11{-}2]_{\mathrm{YSZ}}//[1{-}210]_{\mathrm{saph}} \text{ and } [2{-}1{-}1]_{\mathrm{YSZ}}//[1{-}210]_{\mathrm{saph}}$$

Three variants exist for (001) YSZ grains rotated by 120° following the threefold symmetry of sapphire. While electron diffraction in Fig. 4(a) reveals the coexistence of two possible in-plane orientations (type_a and type_b) of these three variants, XRD azimuthal scans show that one of these two in-plane orientations is promoted, depending on the substrate treatment.

For substrate 1, annealed with nitrogen, the relationship between (001) YSZ and (0001) sapphire is mainly

$$\text{Type_a: } (001)_{\mathrm{YSZ_type_a}}//(0001)_{\mathrm{saph}}:$$

$$[1{-}10]_{\mathrm{YSZ}}//[1{-}210]_{\mathrm{saph}} \text{ and } [1{-}10]_{\mathrm{YSZ}}//[{-}2110]_{\mathrm{saph}}$$

$$\text{and } [1{-}10]_{\mathrm{YSZ}}//[11{-}20]_{\mathrm{saph}} \text{ (Ref. [30])}$$

while for substrate 2, annealed with oxygen, the relationship between (001) YSZ and (0001) sapphire is mainly

$$\text{Type_b: } (001)_{\mathrm{YSZ_type_b}}//(0001)_{\mathrm{saph}}:$$

$$[100]_{\mathrm{YSZ}}//[10{-}10]_{\mathrm{saph}} \text{ and } [100]_{\mathrm{YSZ}}//[0{-}110]_{\mathrm{saph}}$$

$$\text{and } [100]_{\mathrm{YSZ}}//[{-}1100]_{\mathrm{saph}}$$

These three different configurations of YSZ grown on *C*-cut sapphire, (111)YSZ, (001)YSZ_type_a, and (001)YSZ_type_b are presented in Fig. 4(c) with their corresponding electron-diffraction pattern [Fig. 4(a)]. TEM measurements shown in Figs. 4(a) and 4(b) have been performed on 250-nm-thick YSZ layer on substrate 2.

Mismatch values between oxygen lattice of YSZ and first plane of sapphire unit cell have been then determined. The lowest mismatch is reached for (111) YSZ with 0.8% along [11-2]YSZ(111) and [1-210]saph direction (7.8% perpendicularly in-plane). Due to this low mismatch (<1%), the epitaxial growth of YSZ at the interface with sapphire should be driven by this orientation. Then, from the two in-plane orientations of (001) YSZ (orientations type_a and type_b), the lowest mismatch is 1.6% along [1-10]YSZ_type_a and [1-210]saph directions (7.8% perpendicularly in-plane) for the configuration type_a. The configuration type_b presents 2.8% mismatch along [100]YSZ_type_b and [10-10]saph (7.8% perpendicularly in-plane). Furthermore, dark-field (DF) images of YSZ deposited on oxygen-annealed sapphire [Fig. 4(b)] reveal the location of YSZ grains (bright color) corresponding to the different electron-diffraction patterns of Fig. 4(a). We underline here that only a small portion of the YSZ grains are revealed because DF images are only sensitive to one variant of each oriented grain. In agreement with these mismatch values, (111) YSZ is mainly found at the sapphire interface, while (001) YSZ is present either in the upper part of the layer or grown from the interface.

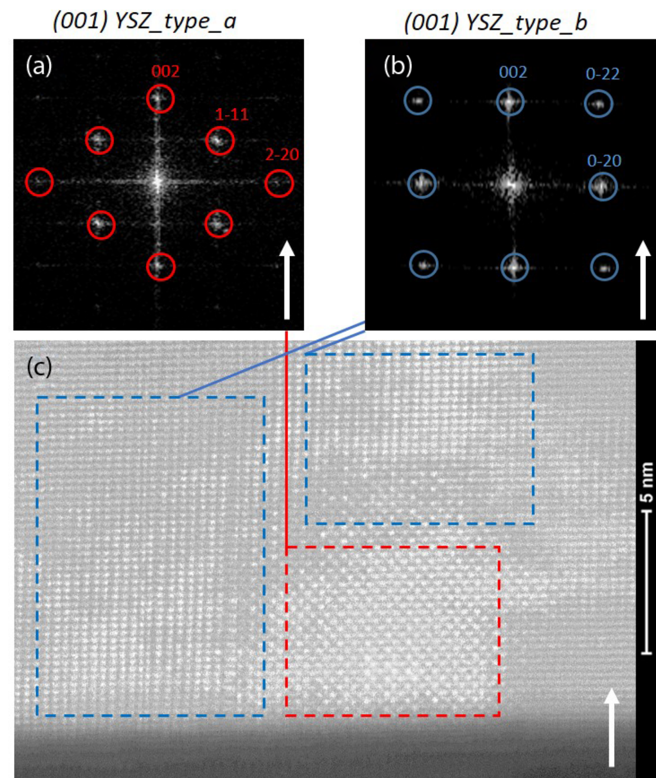

FIG. 5. (a), (b) Fourier transform of the area selected on the cross-sectional HAADF HRSTEM image (c) at the interface of YSZ on oxygen-annealed sapphire (substrate 2). (001)YSZ_type_b nucleus expands vertically and horizontally to cover the (001)YSZ_type_a nucleus. White arrows represent growth axis on Fourier transform (a), (b) and HRSTEM, image (c).

Substrate 1 leads to a growth of (111) YSZ grains from the sapphire interface with (001) YSZ (type_a mainly) only appearing for films thicker than 300 nm (Fig. 3). On substrate 2, (111) YSZ is prohibited or quickly covered with (001) YSZ (type_b mainly) directly growing from the interface (Figs. 4 and 5). This last result is in agreement with the mechanism proposed by Dai *et al.* [30] explaining that both (111) and (001) YSZ nuclei are formed at the interface but, as (001) nuclei growth is faster, coalescence occurs, leading to a stop of the (111) growth. While the analysis of moiré fringes (not shown here) confirms this mechanism, high-resolution STEM (HRSTEM) image of the interface between YSZ and oxygen-annealed sapphire (substrate 2) (Fig. 5) exhibits an additional phenomenon: (001) YSZ type_b nucleus, growing faster from the interface, covers (001) YSZ type_a nucleus after less than 10 nm. This parallel growth mechanism is highlighted with the Fourier transforms Figs. 5(a) and 5(b) obtained from different areas of Fig. 5(c).

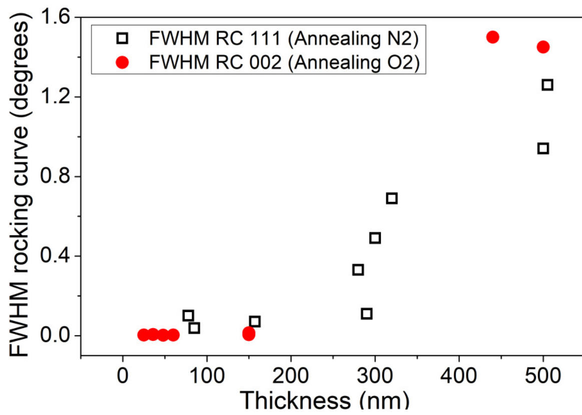

FIG. 6. Full width at half maximum of (111) YSZ and (002) YSZ x-ray diffraction rocking curve peaks as a function of the film thickness for nitrogen-annealed (black squares) and oxygen-annealed (red circles) substrates, respectively.

D. Crystallinity of YSZ

The general quality of thin YSZ films has been determined with AFM and XRD, the mosaicity through the full width at half maximum (FWHM) of the rocking curve of the main XRD peaks. The latter is plotted as a function of the film thickness in Fig. 6. Red circled markers correspond to the oxygen-annealed sapphire with (001) YSZ promoted and black squared markers to the nitrogen-annealed with (111) YSZ promoted. These results exhibit the trend of the rocking curve to be wider for thicker film, for both (111) YSZ and (001) YSZ x-ray diffraction peaks, with a transition around 300-nm-thick films. The sharpest rocking curves of 0.0025° width are obtained on the (002) YSZ x-ray diffraction peak.

For photonic applications, the optical propagation through YSZ requires a film thick enough to guide an optical mode and a crystalline quality high enough to avoid intrinsic propagation losses. To meet the trade-off between thickness and crystalline quality in our YSZ layers, we chose a thickness of 250 nm, which allows guided modes around 1300-nm wavelength. Note that this wavelength is of great interest for Datacom applications, e.g., in big data centers [32]. Considering this thickness, either high-quality (001) or (111)-oriented YSZ films can be grown according to the substrate annealing.

Figure 7(a) presents XRD patterns of both (001) and (111)-oriented YSZ samples used for the demonstration of optical waveguides. Figures 7(b) and 7(c) report the rocking curve of the main peak, (111) YSZ for the substrate annealed with nitrogen (black pattern, sample 1) and (002) YSZ for the substrate annealed with oxygen (red pattern, sample 2). FWHMs of omega scans are 0.0035° and 0.0059° and FWHMs of θ-2θ scans are 0.062° and 0.034° for (111) XRD peak of sample 1 and (002) XRD peak of sample 2, respectively. The rocking curves always comprise a sharp central peak and a broad diffuse background for both YSZ orientations and for different YSZ thicknesses. While the sharp peak can be attributed to YSZ grains well aligned with the *C* plane of sapphire substrate, the broad background probably comes from tilted areas at grain boundaries. These results demonstrate the high quality of both samples, suitable for optical characterizations.

IV. DESIGN, FABRICATION, AND OPTICAL MEASUREMENTS

YSZ is known to be a very hard and resistant material to any kind of dry and wet etchings, hindering the implementation of deeply etched optical waveguides. Moreover, *C*-cut sapphire is also resistant to dicing and no substrate cleavage can be considered, which prevents light injection through the chip facet. To overcome these major limitations, we have implemented rib waveguides, which yield single-mode operation for shallow etch configurations [33] and have developed grating couplers to inject/extract the light from/to cleaved optical fibers through the chip surface, obviating the need for facet preparation.

To ensure single-mode propagation in the waveguides and maximum light injection from grating couplers, finite

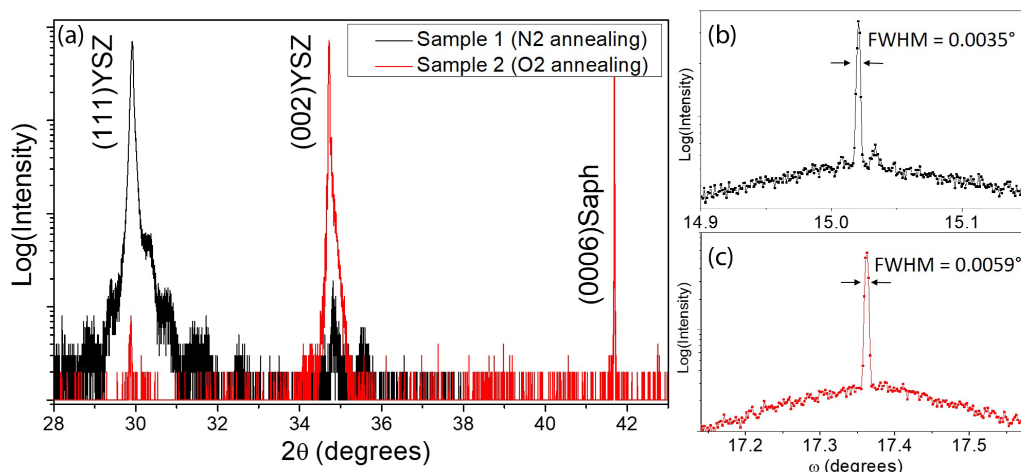

FIG. 7. (a) XRD patterns of 250-nm YSZ thin film on (0001) sapphire in triple-axis configuration. (111) or (001) YSZ has been promoted thanks to the nitrogen (black) or oxygen (red) annealing of substrate 1 and 2, respectively. FWHM (2θ) of main peaks are in $10^{-2°}$ range. (b), (c) Rocking curves of the main YSZ XRD peak of sample 1 (111) YSZ and sample 2 (002) YSZ. FWHM (ω) of rocking curves are in the $10^{-3°}$ range.

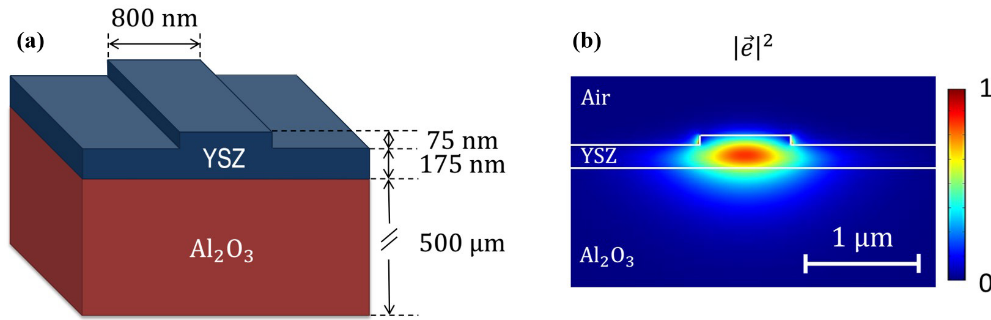

FIG. 8. (a) Schematic view of the rib waveguides designed, fabricated, and optically characterized: 250-nm YSZ total thickness, 75-nm depth etched, and 800-nm waveguide width. (b) FDTD simulations of TE mode propagation of YSZ ($n = 2.15$) on sapphire ($n = 1.75$) at 1300-nm wavelength.

difference time domain (FDTD) simulations have been performed. Considering the already discussed film quality and a refractive index of 2.15 measured by spectroscopic ellipsometry at 1350-nm wavelength, YSZ thickness of $H = 250$ nm, etching depth of $T = 75$ nm, and width of $W = 800$ nm have been targeted for the fabrication (Fig. 8). For the grating couplers, we chose a pitch of 1 μm with a duty cycle of 50%, resulting in central wavelength of 1380 nm for an angle of 20°.

Electron-beam lithography and ion-beam etching (IBE) have been used to pattern optical waveguides. YSZ is an insulator and, to avoid large charging effect during the lithography, a thin layer of gold on top of the electronic resist (hydrogen silsesquioxane) was deposited. The optimization of the IBE etching has been carried out varying parameters including accelerating tension and atmosphere during etching to reach etching depth of 75 nm. Several waveguide lengths from 400 μm to 6 mm have been fabricated and tested to determine the propagation loss of the guided mode injected/collected via grating couplers.

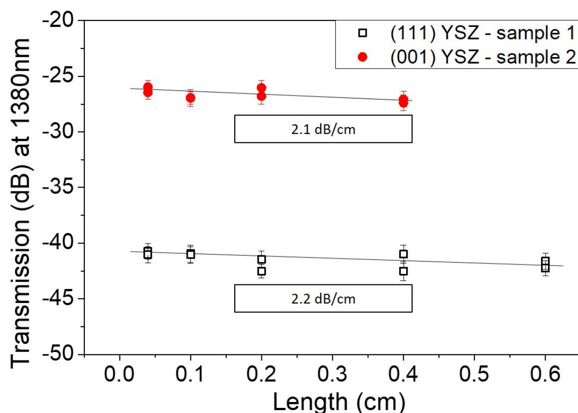

FIG. 9. Fiber-to-chip transmission measurements of rib waveguides (grating couplers injection) for the two promoted orientations of YSZ. Sample 1 (nitrogen-annealed substrate) and sample 2 (oxygen-annealed substrate) as a function of the waveguide lengths from 400 μm to 6 mm. Propagation loss of about 2 dB/cm was obtained for both orientations. The different intercepts of the fitting lines are due to different power injection levels through the grating couplers.

Optical loss measurements have finally been performed at 1380 nm (Fig. 9). Both sample 1 [(111)-oriented YSZ] and sample 2 [(001)-oriented YSZ] exhibited propagation losses as low as 2 dB/cm. These values demonstrate the potential of the YSZ platform for the development of integrated photonic circuits [5,34].

V. CONCLUSION

A complete study of the growth of (001) YSZ and (111) YSZ layers on *C*-cut sapphire has been presented, based on careful x-ray diffraction and transmission electron microscopy measurements. The annealing of sapphire substrates has a strong effect on the YSZ crystal orientations. Indeed, a thermal annealing under oxygen atmosphere promoted a (001) growth of YSZ for film thicknesses from 50 to 500 nm, while an annealing with nitrogen led to a growth of (111) YSZ for films up to 300-nm height.

For both orientations, high-quality YSZ films have been obtained with rocking curve width as narrow as $10^{-3°}$. Furthermore, a simple mismatch-based mechanism has been proposed to explain the different in-plane orientations of YSZ on sapphire. Then, photonic structures such as input and output fiber-to-chip grating couplers and rib waveguides have been designed, fabricated, and characterized. Finally, propagation loss as low as 2 dB/cm has been demonstrated for both (111) YSZ- and (001) YSZ-based waveguides. These results are thus very promising and open a route for the integration of functional oxides in photonics.

ACKNOWLEDGMENTS

This project has received funding from the European Research Council (ERC) under the European Union's Horizon 2020 research and innovation program (ERC POPSTAR - Grant Agreement No. 647342) and the French Industry Ministry Nano2017 program. The authors also acknowledge C2N Nanocenter of the French RENATECH network where the devices were fabricated, ANR "Investissement d'Avenir" program (10-EQPX-0050) for having funded the acquisition of the NANOTEM platform (Dual-beam FIB-FEG FEI SCIOS system and TEM-STEM FEI Titan Themis) used in this work.

[1] W. N. Ye and Y. Xiong, J. Mod. Opt. **60**, 1299 (2013).
[2] D. Thomson, A. Zilkie, J. E. Bowers, T. Komljenovic, G. T. Reed, L. Vivien, Delphine Marris-Morini, E. Cassan, L. Virot, J.-M. Fédéli, J.-M. Hartmann, J. H. Schmid, Dan-Xia Xu, F. Boeuf, P. O'Brien, G. Z. Mashanovich, and M. Nedeljkovic, J. Opt. **18**, 073003 (2016).
[3] Z. Fang and C. Z. Zhao, Int. Sch. Res. Notices **2012**, 428690 (2012).
[4] P. Rojo Romeo, X. Hu, S. Cueff, B. Wague, R. Orobtchouk, B. Vilqui, R. Bachelet, G. Grenet, C. Dubourdieu, P. Regreny, G. Saint-Girons, P. Castera, A. M. Gutierrez, N. Sanchez, T. Angelova, P. Sanchis, S. Abel, and J. Fompeyrine, in *Proceedings of the 17th International Conference on Transparent Optical Networks (ICTON), Budapest* (IEEE, 2015), pp. 1–4.
[5] F. Eltes, D. Caimi, F. Fallegger, M. Sousa, E. O'Connor, M. D. Rossell, B. Offrein, J. Fompeyrine, and S. Abel, ACS Photonics **3**, 1698 (2016).
[6] S. Abel, T. Stöferle, C. Marchiori, C. Rossel, M. D. Rossell, R. Erni, D. Caimi, M. Sousa, A. Chelnokov, B. J. Offrein, and J. Fompeyrine, Nat. Commun. **4**, 1671 (2013).
[7] M. J. Dicken, K. Diest, Y.-B. Park, and H. A. Atwater, J. Cryst. Growth **300**, 330 (2007).
[8] A. Guarino, G. Poberaj, D. Rezzonico, R. Degl'Innocenti, and P. Günter, Nat. Photonics **1**, 407 (2007).
[9] L. Méchin, J.-C. Villégier, G. Rolland, and F. Laugier, Physica C: Supercond. **269**, 124 (1996).
[10] X. D. Wu, R. E. Muenchausen, N. S. Nogar, A. Pique, R. Edwards, B. Wilkens, T. S. Ravi, D. M. Hwang, and C. Y. Chen, Appl. Phys. Lett. **58**, 304 (1991).
[11] L. F. Chen, P. F. Chen, L. Li, S. L. Li, X. N. Jing, S. J. Pan, and Y. H. Guo, Appl. Phys. Lett. **61**, 2412 (1992).
[12] D. H. Kim, N. M. Aimon, X. Y. Sun, L. Kornblum, F. J. Walker, C. H. Ahn, and C. A. Ross, Adv. Funct. Mater. **24**, 5889 (2014).
[13] C. López-Gándara, F. M. Ramos, and A. Cirera, J. Sensors **2009**, 258489 (2009).
[14] T. Falcade and C. de Fraga Malfatti, in *Electrochemical Cells – New Advances in Fundamental Researches and Applications*, edited by Y. Shao (InTech, Rijeka, Croatia, 2012).
[15] B. A. Boukamp, Nat. Mater. **2**, 294 (2003).
[16] N. Q. Minh, Solid State Ionics **174**, 271 (2004).
[17] B. Scherrer, S. Heiroth, R. Hafner, J. Martynczuk, A. Bieberle-Hütter, J. L. M. Rupp, and L. J. Gauckler, Adv. Funct. Mater. **21**, 3967 (2011).
[18] S. K. Pandey, O. P. Thakur, R. Raman, A. Goyal, and A. Gupta, Appl. Surf. Sci. **257**, 6833 (2011).
[19] G. Stapper, M. Bernasconi, N. Nicoloso, and M. Parrinello, Phys. Rev. B **59**, 797 (1999).
[20] Y.-N. Xu, Z.-q. Gu, and W. Y. Ching, Phys. Rev. B **56**, 14993 (1997).
[21] J. Joo and G. Choi, Solid State Ionics **177**, 1053 (2006).
[22] D. E. Ruddell, B. R. Stoner, and J. Y. Thompson, Thin Solid Films **445**, 14 (2003).
[23] P. Camagni, P. Galinetto, G. Samoggia, and N. Zema, Solid State Commun. **83**, 943 (1992).
[24] A. V. Butashin, V. P. Vlasov, V. M. Kanevskii, A. E. Muslimov, and V. A. Fedorov, Crystallogr. Rep. **57**, 824 (2012).
[25] I. Vilfan, F. Lançon, and J. Villain, Surf. Sci. **392**, 62 (1997).
[26] K. G. Saw, J. Mater. Sci. **39**, 2911 (2004).
[27] M. Pollnau, J. D. B. Bradley, F. Ay, E. H. Bernhardi, R. M. de Ridder, and K. Wörhoff, Proc. SPIE **7605**, 76050M (2010).
[28] H. M. Christen and G. Eres, J. Phys.: Condens. Matter **20**, 264005 (2008).
[29] A. Infortuna, A. S. Harvey, and L. J. Gauckler, Adv. Funct. Mater. **18**, 127 (2008).
[30] J. Y. Dai, H. C. Ong, and R. P. H. Chang, J. Mater. Res. **14**, 1329 (1999).
[31] D. K. Fork, D. B. Fenner, G. A. N. Connell, J. M. Phillips, and T. H. Geballe, Appl. Phys. Lett. **57**, 1137 (1990).
[32] D. Marris-Morini, L. Virot, C. Baudot, J.-M. Fédéli, G. Rasigade, D. Perez-Galacho, J.-M. Hartmann, S. Olivier, P. Brindel, P. Crozat, F. Bœuf, and L. Vivien, Opt. Express **22**, 6674 (2014).
[33] R. A. Soref, J. Schmidtchen, and K. Petermann, IEEE J. Quantum Electron. **27**, 1971 (1991).
[34] J. F. Bauters, M. L. Davenport, M. J. R. Heck, J. K. Doylend, A. Chen, A. W. Fang, and J. E. Bowers, Opt. Express **21**, 544 (2013).